Packet Error Probability and Effective Throughput for Ultra-reliable and Low-latency UAV Communications

Kezhi Wang, Cunhua Pan, Hong Ren, Wei Xu, Lei Zhang and Arumugam, Nallanathan, *Fellow, IEEE*

Abstract

In this paper, we study the average packet error probability (APEP) and effective throughput (ET) of the control link in unmanned-aerial-vehicle (UAV) communications, where the ground central station (GCS) sends control signals to the UAV that requires ultra-reliable and low-latency communications (URLLC). To ensure the low latency, short packets are adopted for the control signal. As a result, the Shannon capacity theorem cannot be adopted here due to its assumption of infinite channel blocklength. We consider both free space (FS) and 3-Dimensional (3D) channel model by assuming that the locations of the UAV are randomly distributed within a restricted space. We first characterize the statistical characteristics of the signal-to-noise ratio (SNR) for both FS and 3D model. Then, the closed-form analytical expressions of APEP and ET are derived by using Gaussian-Chebyshev quadrature. Also, the lower and upper bounds are derived to obtain more insights. Finally, we show the solutions to obtain the sub-optimal value of packet length numerically with the objective of maximizing the ET. Our analytical results are verified by the Monte-Carlo simulations.

Keywords – UAV, URLLC, packet error probability, short packet transmission

I. Introduction

Unmanned aerial vehicle (UAV) communication has attracted increasingly attention from both industry and academia [1], [2]. Compared with the conventional terrestrial communications, UAV can be deployed in a swift and flexible way on demands. For example, it can be used to offload heavy data load in hot spot area, and provide temporary communication services when public communication infrastructure is damaged due to nature disasters. In addition, UAV can act as a

K. Wang (kezhi.wang@northumbria.ac.uk) is with the department of Computer and Information Sciences, Northumbria University, UK; C. Pan, H. Ren and A. Nallanathan are with School of Electronic Engineering and Computer Science, Queen Mary University of London, London, E1 4NS, U.K. (Email:{c.pan, h.ren, a.nallanathan}@qmul.ac.uk), W. Xu (wxu@seu.edu.cn) is with NCRL, Southeast University, Nanjing, China, L. Zhang is with School of Engineering, University of Glasgow, Glasgow, G12 8QQ, U.K (Lei.Zhang@glasgow.ac.uk).

relay when there is no reliable direct communication links between distant nodes. The channel quality between the UAV and ground users can be enhanced due to the higher probability of short-distance line-of-sight (LoS) links.

UAV trajectory design has been studied in [3]–[5]. In particular, Zeng *et al.* studied the throughput maximization problem by jointly optimizing transmission power and UAV trajectory for mobile relay system. The energy consumption of fixed-wing UAVs was derived in [4], based on which energy efficiency was maximized subject to the constraints of UAV speed and acceleration. Then, Wu *et al.* extended [3], [4] to a multi-UAV enabled communication system, and the fairness issue was studied by jointly optimizing user association, UAV trajectory and power control. The other research line is UAV location/placement optimization for static-UAV enabled wireless networks [6]–[8]. Specifically, Hourani *et al.* [6] provided an analytical approach to optimize the altitude of UAV to provide maximum radio coverage on ground users. The circle packing theory was adopted in [7] to optimize the locations of multiple UAVs. Alzenad *et al.* [8] proposed an optimal placement algorithm for maximizing the number of covered users using the minimum transmit power. Moreover, UAV combined with mobile edge computing has been reported in [9].

However, all the above works mainly focused on the conventional data transmission without considering the control communication links which require much more stringent latency and higher reliability in order to avoid collision and crash. The control communication link generally requires low data rate for exchanging safety-critical signals. To ensure the extremely low latency (e.g., 1 ms), short packet (e.g., 20 bytes) should be adopted [10]. Thus the Shannon capacity formula based on the philosophy of the law of large numbers does not guarantee an asymptotically reliable communication. Therefore non-negligible packet error probability exists and effective throughput may drop. In [11], the authors derived the maximum range between UAVs and a ground control station such that the transmission delay and the overall packet loss probability requirement can be guaranteed. In [12], the UAV serves as a relay to provide URLLC services between the controller and the robot. However, there is a paucity of contributions devoted to the performance analysis in UAV-URLLC communication systems. In [13], the approximate closed-form expression of the packet error probability in finite blocklength regime has been derived, which is an involved function of packet length/channel uses, signal-to-noise ratio (SNR) and packet size. This calls for a complete paradigm shift to the study of average packet error probability performance (APEP) and effective throughput (ET) in UAV communications.

Against the above background, the contributions of this paper are summarised as follows:

1) We characterize the statistical characteristics of the signal-to-noise ratio (SNR) for both free space (FS) and 3-dimensional (3D) model by assuming that the UAV is assumed to fly freely in a restricted area. We consider the randomness of the locations of UAV by using the stochastic geometry theory. Both FS and 3D channel model are considered, where FS is used for the environment where the line-of-sight (LoS) dominates, whereas 3D model is applied to the scenario where the None Los (NLoS) cannot be ignored such as urban areas.
2) We then study the average packet error probability (APEP) and effective throughput (ET) under short packet transmission of the control link from ground control station (GCS) to UAV. The Gaussian-Chebyshev quadrature method is adopted to derive the closed-form expression of APEP and ET under short packet transmission, which can provide engineering insights on the packet size design and more understanding of the packet error rate incurred in transmission.
3) Then, closed-form lower bounds are derived for APEP and ET under both FS and 3D channel model by using the convexity of error expression and Jensen's inequality. Also, upper bound is derived for APEP and ET under FS model with insights given to the practical system design.
4) Moreover, the sub-optimal value of packet length with the objective of maximizing the ET under FS and 3D is provided.
5) Monte-Carlo simulations are conducted to demonstrate the correctness of our derived results, and show the tightness of the analytical expressions under different conditions.

The rest of this paper is organized as follows. In Section II, we first introduce the system model including FS, 3D channel model and the point-to-point short packet transmission theory. In Section III, the exact, lower bound and upper bound are derived for APEP and ET under FS channel model, whereas the exact and lower bound are studied for APEP and ET under 3D channel model in Section IV. Also, the sub-optimal value of packet length with the objective of maximizing the ET under FS and 3D are shown in Section III and IV, respectively. Simulation results and analysis are shown in Section V. Finally, the paper is concluded in Section VI.

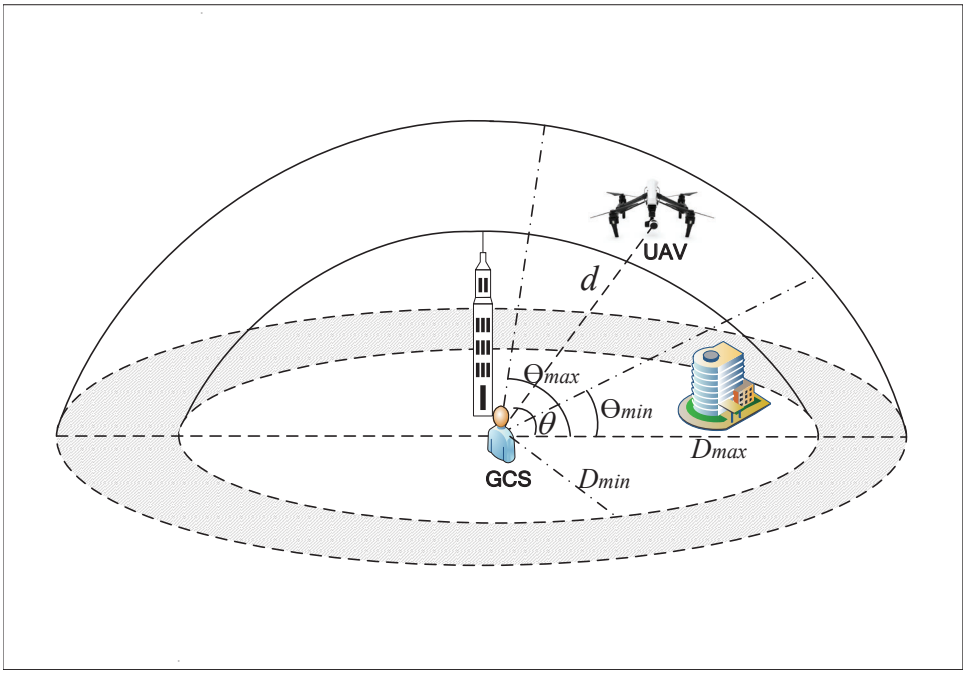

Fig. 1: Illustration of the low-latency transmission of control information from GCS to a UAV.

II. System Model

We consider a UAV communication network where a GCS sends remote control signals to a UAV, which has stringent QoS requirements in terms of ultra-high reliability and ultra-low latency, as shown in Fig. 1. For simplicity, both GCS and UAV are assumed to be equipped with one antenna. The GCS is also assumed to be located at the center of the sphere. Two hemispheres are introduced that share the same center point at the GCS. The UAV is assumed to be within the outer hemisphere to ensure that the UAV is within the control range of the GCS. In addition, we assume that the UAV will not fly into the inner hemisphere. The assumption is reasonable since there may be some obstacles or buildings around the GCS. The radius of the inner and outer hemisphere are denoted as D_{min} and D_{max}, respectively. The UAV is assumed to fly freely within the space specified by the two hemispheres as shown in Fig. 1. Then, we can assume that the UAV is uniformly distributed in this space, and the cumulated distribution function (CDF) of d can be calculated as [14]

$$F_d(x) = \begin{cases} \frac{x^3 - D_{min}^3}{D_{max}^3 - D_{min}^3}, & D_{min} \le x \le D_{max}, \\ 1, & x > D_{min}. \end{cases} \tag{1}$$

and the probability distribution function (PDF) of d is

$$f_d(x) = \begin{cases} \frac{dF_d(x)}{dx} = \frac{3x^2}{D_{max}^3 - D_{min}^3}, & D_{min} \leq x \leq D_{max}, \\ 0, & \text{otherwise.} \end{cases} \tag{2}$$

A. Channel model

Two channel models are considered as follows:

1) Free-space (FS) Channel Model: This channel is the simplest channel model, which is for the scenario where the LoS dominates the environment, i.e., in less crowded areas. The channel gain from the GCS to the UAV mainly depends on the GCS-UAV distance and the antenna gain. Then, the channel power gain from GCS to UAV follows the FS path loss model, which can be expressed as $h = \beta d^{-2}$ [15], where d is the GCS-UAV distance and β is the channel power at the reference distance of $d = 1$ m that is related to the antenna gain. This channel model is valid when the UAV is deployed in an obstacle-free area, such as big square, play ground, large lawn, etc. We assume that the transmission power from the GCS to the UAV is fixed as P and the noise power at the UAV is denoted as σ^2. Then, the SNR at UAV is given by

$$\gamma^{FS} = \lambda d^{-2} \tag{3}$$

where $\lambda = P\beta/\sigma^2$.

2) 3D Channel Model: We adopt the 3D channel model proposed in [6] which is more practical than the above free space channel model for urban areas with dense obstacles such as buildings and trees. In this model, both line-of-sight (LoS) and non line-of-sight links are considered. The probability of having a LoS connection between the GCS and the UAV is given by [6]

$$P_{\text{LoS}} = \frac{1}{1 + a\exp\left(-b\left(\theta - a\right)\right)}, \tag{4}$$

where a and b are positive constants that depend on the environment and the values are given in [6], θ is the elevation angle given by $\theta = \arctan\frac{h}{g}$ [1] with h denoting the altitude of the UAV and g horizontal distance between the UAV and the GCS. The probability of NLoS is $P_{\text{NLoS}} = 1 - P_{\text{LoS}}$. Also, one can get the PDF of θ as

$$f_\theta(x) = \frac{1}{\Theta_{max} - \Theta_{min}} \tag{5}$$

[1] θ here means the degrees of the angle and its value ranges from 0 to 90.

and the CDF of θ as

$$F_\theta(x) = \frac{x - \Theta_{min}}{\Theta_{max} - \Theta_{min}}. \tag{6}$$

The channel path loss models for LoS and NLoS links shown in dB are [6]

$$L_{\mathrm{k}} = 20\log_{10}\left(\frac{4\pi f_c d}{c}\right) + \eta_{\mathrm{k}}, \mathrm{k} \in \{\mathrm{LoS}, \mathrm{NLoS}\} \tag{7}$$

where the first term corresponds to the free space path loss, and η_{LoS} and η_{NLoS} are the additional losses for LoS and NLoS, respectively. In general, η_{NLoS} is much larger than η_{LoS} due to the severe path loss of NLoS. Then, for a given location of UAV, we consider the mean path loss by considering the probability of both LoS and NLoS links:

$$L(\theta, d) = L_{\mathrm{LoS}} P_{\mathrm{LoS}} + L_{\mathrm{NLoS}} P_{\mathrm{NLoS}}. \tag{8}$$

By substituting (4) and (7) into (8), the mean path loss in (8) can be rewritten as

$$L(\theta, d) = \frac{A}{1 + a\exp\left(-b\left(\theta - a\right)\right)} + 20\log_{10}\left(d\right) + C, \tag{9}$$

where A and C are constants given by $A = \eta_{\mathrm{LoS}} - \eta_{\mathrm{NLoS}}$ and $C = 20\log_{10}\left(\frac{4\pi f_c}{c}\right) + \eta_{\mathrm{NLoS}}$, respectively.

Assume that the transmission power from GCS to UAV is fixed as P and the noise power at UAV is denoted as σ^2, then the signal-to-noise ratio (SNR) at the UAV is given by [14] [6]

$$\begin{aligned} \gamma^{3D} &= \frac{P}{\sigma^2} 10^{-\frac{L(\theta,d)}{10}} \\ &= \tilde{C} d^{-2} e^{\frac{\tilde{A}}{1+a\exp(-b(\theta-a))}} \\ &= \hat{d}\hat{\theta} \end{aligned} \tag{10}$$

where $\hat{d} = \tilde{C} d^{-2}$, $\hat{\theta} = e^{\frac{\tilde{A}}{1+a\exp(-b(\theta-a))}}$, $\tilde{A} = -A\frac{\ln 10}{10} > 0$ and $\tilde{C} = \frac{P}{\sigma^2} e^{-\frac{C\ln 10}{10}}$.

B. Point-to-point Short Packet Transmission Theory

Let us define the coding rate, R, as the ratio of the number of information bits to the total number of bits per channel use. According to [16], the Shannon capacity is defined as the maximum coding rate for which an arbitrarily low packet error probability is achievable for a sufficiently large number of codewords. However, for the control signal transmission, the packet length, or the number of codewords, should be small to ensure the stringent latency requirement.

Thus, the Shannon capacity theorem may not guarantee an success transmission and the packet error probability cannot be ignored.

We assume that the packet size of the control signal is L bits, which should be transmitted within $T_{\max}$ seconds. Then, the number of bits per channel use is given by $M = BT_{\max}$ [17], where B denotes the system bandwidth. Thus, the coding/data rate is given by $R = L/M$. According to [17], a very tight approximation of the packet error probability for a point-to-point transmission under finite blocklength transmission region is given by

$$\varepsilon(\gamma^+) = Q\left(f\left(\gamma^+\right)\right), \tag{11}$$

where γ^+ can be either γ^{FS} or γ^{3D}, $f\left(\gamma^+\right) = \sqrt{\frac{M}{V(\gamma^+)}}\left(\ln(1+\gamma^+) - R_s\right)$, $R_s = \frac{L\ln 2}{M}$ (nats per channel use, or npcu), $V(\gamma^+)$ is the channel dispersion that is given by $V(\gamma^+) = 1-(1+\gamma^+)^{-2}$ [13], and $Q\left(x\right)$ is the Gaussian Q-function given by $Q\left(x\right) = \frac{1}{\sqrt{2\pi}}\int_x^\infty e^{-\frac{t^2}{2}}\mathrm{d}t$. The expression of (11) can be interpreted as follows: ε is minimum packet error probability for which there exists an encoder/decoder pair to transmit L information bits within M bits per channel use.

Also, the ET can be given by

$$H(\gamma^+) = R_s\left(1-\varepsilon(\gamma^+)\right). \tag{12}$$

In the following, we will derive the APEP and ET by considering the randomness of the UAV location in the restricted area, under both FS and 3D scenarios. The complicated expression of ε in (11), especially the expression of $V(\gamma^+)$, makes the analysis of APEP and ET a challenging task. Next, the APEP and ET are derived for FS and 3D channel model in Section III and IV, respectively.

III. APEP and ET under Free-Space Channel Model

A. *PDF of* γ^{FS}

In this section, we aim to derive the APEP under free-space channel model by transmitting a packet with fixed size of L. Specifically, the APEP in this case is defined as

$$\bar{\varepsilon}^{FS} = \mathbb{E}\{\varepsilon(\gamma^{FS})\} = \int_{D_{min}}^{D_{max}} \varepsilon(\gamma^{FS}) f_d(x) dx, \tag{13}$$

where $f_d(x)$ is the PDF of d that can be obtained from (1), and γ^{FS} in $\varepsilon(\gamma^{FS})$ is provided in (3) and (11) respectively.

Then, the ET is given by

$$\bar{H}^{FS} = \mathbb{E}(R_s\left(1-\gamma^{FS}\right)) = R_s\left(1-\bar{\varepsilon}^{FS}\right). \tag{14}$$

To reduce the analysis complexity, we consider the PDF of γ^{FS} in the following lemma.

Lemma 1: The PDF of SNR γ^{FS} denoted as $f_{\gamma^{FS}}(x)$ is given by [14]

$$f_{\gamma^{FS}}(x) = \begin{cases} \frac{3x^{-\frac{5}{2}}\lambda^{3/2}}{2(D_{max}^3 - D_{min}^3)}, \gamma_{min}^{FS} \leq x \leq \gamma_{max}^{FS} \\ 0, \qquad \text{otherwise}, \end{cases} \tag{15}$$

where $\gamma_{min}^{FS} = \frac{\lambda}{D_{max}^2}$ and $\gamma_{max}^{FS} = \frac{\lambda}{D_{min}^2}$.

Proof: Please refer to Appendix A. ■

Moreover, when $D_{min} = 0$, one has $f_{\gamma^{FS}}(x) = \frac{3x^{-\frac{5}{2}}(\lambda^{FS})^{3/2}}{2D_{max}^3}, x \geq \gamma_{min}^{FS}$. This can be seen as the case where there is no obstacle between the control centre and UAV and also, UAV may fly back to the control centre.

B. Chebyshev Approximation

By using (11) and (15), APEP can be re-expressed as

$$\begin{aligned} \bar{\varepsilon} &= \int_{\gamma_{min}^{FS}}^{\gamma_{max}^{FS}} Q\left(\sqrt{\frac{M}{V(x)}}\left(\ln(1+x) - R_s\right)\right) f_{\gamma^{FS}}(x)dx \\ &= \frac{3\lambda^{3/2}}{4(D_{max}^3 - D_{min}^3)} \cdot \int_{\gamma_{min}^{FS}}^{\gamma_{max}^{FS}} \text{erfc}\left(\frac{1}{\sqrt{2}}\sqrt{\frac{M}{V(x)}}\left(\ln(1+x) - R_s\right)\right) x^{-\frac{5}{2}}dx, \end{aligned} \tag{16}$$

where γ_{min}^{FS} and γ_{max}^{FS} are given in Lemma 1, and the last equality follows by using the relationship of $\text{erfc}(x) = 2Q(\sqrt{2}x)$. To the best of our knowledge, it is very difficult to find the closed-form expression of (16), if not impossible.

Next, we apply Gaussian-Chebyshev quadrature to address this issue by using [18, Eq. (25.4.30)]. Let us first define

$$q^{FS}(x) = \text{erfc}\left(\frac{1}{\sqrt{2}}\sqrt{\frac{M}{V(x)}}\left(\ln(1+x) - R_s\right)\right) x^{-\frac{5}{2}}. \tag{17}$$

Then, one can have

$$\int_{\gamma_{min}^{FS}}^{\gamma_{max}^{FS}} q^{FS}(x)dx \approx \frac{\gamma_{max}^{FS} - \gamma_{min}^{FS}}{2} \sum_{i=1}^{N} a_i \cdot q^{FS}\left(\frac{\gamma_{max}^{FS} - \gamma_{min}^{FS}}{2} t_i + \frac{\gamma_{max}^{FS} + \gamma_{min}^{FS}}{2}\right), \tag{18}$$

where t_i is the i-th zero of Legendre polynomials, N is the number of terms, a_i is the Gaussian weight given by Table (25.4) of [18]. By substituting (18) into (16), one can have

$$\bar{\varepsilon}^{FS} \approx \frac{3\lambda^{3/2}(\gamma_{max}^{FS}-\gamma_{min}^{FS})}{8(D_{max}^3-D_{min}^3)} \sum_{i=1}^{N} a_i \cdot q^{FS}\left(\frac{\gamma_{max}^{FS}-\gamma_{min}^{FS}}{2}t_i + \frac{\gamma_{max}^{FS}+\gamma_{min}^{FS}}{2}\right) \triangleq \bar{\varepsilon}_C^{FS}. \tag{19}$$

With the increase of N, the accuracy of the above expression will be increased, but at the cost of more computations. To obtain more insights, we derive the approximate expression of $\bar{\varepsilon}$ in the following section.

Then, by using (19) and (14), one can get the ET as

$$\bar{H}_C^{FS} = R_s\left(1-\bar{\varepsilon}^{FS}\right). \tag{20}$$

C. Lower Bound

In the following, we aim to derive the lower bound of the APEP in FS channel model in closed form. To this end, we first introduce the following lemma.

Lemma 2: $\varepsilon(\gamma^+)$ is a convex function of γ^+.

Proof: Please refer to Appendix B. ■

According to Lemma 2, by employing the Jensen's inequality, we can obtain the lower bound of APEP as follows:

$$\bar{\varepsilon}^{FS} = \mathbb{E}\{\varepsilon(\gamma^{FS})\} \geq \varepsilon(\mathbb{E}\{\gamma^{FS}\}) \triangleq \bar{\varepsilon}_{\mathrm{LB}}^{FS}. \tag{21}$$

To obtain $\bar{\varepsilon}_{\mathrm{LB}}^{FS}$, we only need to calculate $\mathbb{E}\{\gamma^{FS}\}$, which is much easier than directly calculating $\bar{\varepsilon}^{FS}$.

By using (15), one can get $\mathbb{E}\{\gamma^{FS}\}$ as

$$\begin{aligned}\mathbb{E}\{\gamma^{FS}\} &= \int_{\gamma_{min}^{FS}}^{\gamma_{max}^{FS}} f_{\gamma^{FS}}(x)x dx \\ &= \int_{\gamma_{min}^{FS}}^{\gamma_{max}^{FS}} \frac{3\lambda^{3/2}x^{-\frac{5}{2}}\cdot x}{2(D_{max}^3-D_{min}^3)}dx \\ &= \frac{3\lambda^{3/2}}{\sqrt{\gamma_{max}^{FS}}\,(D_{max}^3-D_{min}^3)} - \frac{3\lambda^{3/2}}{\sqrt{\gamma_{min}^{FS}}\,(D_{max}^3-D_{min}^3)}\end{aligned} \tag{22}$$

Then, by using (11) and (21), $\bar{\varepsilon}_{\mathrm{LB}}^{FS}$ can be written as

$$\bar{\varepsilon}_{\mathrm{LB}}^{FS} = \varepsilon\left(\frac{3\lambda}{D_{max}^2+D_{min}^2+D_{max}D_{min}}\right). \tag{23}$$

Similarly, ET can be expressed as

$$\begin{aligned}\bar{H}_{LB}^{FS} &= R_s\left(1-\bar{\varepsilon}_{LB}^{FS}\right)\\ &= R_s\left(1-\varepsilon\left(\frac{3\lambda}{D_{max}^2+D_{min}^2+D_{max}D_{min}}\right)\right).\end{aligned} \tag{24}$$

Remark 1: When $\lambda \gg 1$ (i.e., $P/\sigma^2 \gg 1$), $\bar{\varepsilon}_{\mathrm{LB}}^{FS}$ in (23) can be further simplified as

$$\bar{\varepsilon}_{\mathrm{LB}}^{FS} = Q\left(\sqrt{M}\left(\ln\left(K^F\lambda\right)-R_s\right)\right), \tag{25}$$

where $K^F = \frac{3}{D_{max}^2+D_{min}^2+D_{max}D_{min}}$. Then, one can see that the APEP decreases proportionally with the increase of $Q\left(\sqrt{M}(\ln(K^F\lambda))\right)$, i.e., M or λ. .

Proof: Please refer to Appendix C. ■

Remark 2: When $\lambda \gg 1$ (i.e., $P/\sigma^2 \gg 1$), one can have $\bar{H}_{LB}^{FS} \to R_s$.

Proof: Please refer to Appendix D. ■

D. Upper Bound

In this section, we provide the upper bound of APEP, which is especially tight in high SNR region when $\lambda \gg 1$.

By using (60) and (61), (16) can be approximated as

$$\begin{aligned}\bar{\varepsilon}_{\mathrm{UB}}^{FS} =& \frac{3\lambda^{3/2}}{4(D_{max}^3-D_{min}^3)}\cdot\int_{\gamma_{min}^{FS}}^{\gamma_{max}^{FS}}\mathrm{erfc}\left(\frac{\ln 2\cdot\sqrt{M}}{\sqrt{2}}\left(\log_2(x)-\frac{L}{M}\right)\right)x^{-\frac{5}{2}}dx\\ =& \frac{3\lambda^{3/2}}{4(D_{max}^3-D_{min}^3)}\left(u(\gamma_{max}^{FS})-u(\gamma_{min}^{FS})\right),\end{aligned} \tag{26}$$

where the last equality is obtained by variable substitution and using [19], [20], and function $u(x)$ is given by

$$u(x) = -\frac{2\mathrm{erfc}\left(\frac{M\ln x - L\ln 2}{\sqrt{2}\sqrt{M}}\right)}{3x^{3/2}} - \frac{2}{3}e^{\frac{(L\ln 4-3)^2-4L^2\ln^2(2)}{8M}}\cdot\mathrm{erf}\left(\frac{-L\ln 4+2M\ln x+3}{2\sqrt{2}\sqrt{M}}\right). \tag{27}$$

Remark 3: One can further approximate (26) as

$$\begin{aligned}\bar{\varepsilon}_{\mathrm{UB}}^{FS} \approx& \frac{D_{max}^3}{2\left(D_{max}^3-D_{min}^3\right)}\left(\mathrm{erfc}\left(\frac{M\ln\left(\frac{\lambda}{D_{max}^2}\right)-L\ln(2)}{\sqrt{2M}}\right)-\right.\\ &\left.\mathrm{erfc}\left(\frac{M\ln\left(\frac{\lambda}{D_{min}^2}\right)-L\ln(2)}{\sqrt{2M}}\right)\right).\end{aligned} \tag{28}$$

Then, one can get the insights that APEP increases with the increase of L, with other parameters fixed.

Proof: Please refer to Appendix E. ■

E. Throughput Maximization

In this section, we consider the throughput maximization problem under the latency constraint as follows

$$\begin{aligned} \mathcal{P}1: \ & \max_{M} \quad \bar{H}^{FS} \\ & \text{subject to}: M_{min} \leq M \leq M_{max}. \end{aligned} \tag{29}$$

One can see that the above optimization can be transformed as

$$\begin{aligned} & \max_{M} \quad \bar{H}^{FS}_{LB} \\ & \text{subject to}: M_{min} \leq M \leq M_{max} \end{aligned} \tag{30}$$

Proof: It is obvious that maximizing $\bar{H}^{FS}$ may be equivalent to maximizing its lower bound. ■

By using (25), one can get $\bar{H}^{FS}_{LB}$ as

$$\bar{H}^{FS}_{LB} = R_s \left(1 - Q\left(\sqrt{M}\left(\ln\left(K^F\lambda\right) - R_s\right)\right)\right). \tag{31}$$

Then, by taking the first-order derivative of $\bar{H}^{FS}_{LB}$ with respect to M, one can have

$$\begin{aligned} \frac{\partial \bar{H}^{FS}_{LB}(M)}{\partial M} = \frac{L\ln 2}{2M^2}\Bigg(&\text{erfc}\left(\frac{M\ln\left(K^F\lambda\right) - L\ln 2}{\sqrt{2M}}\right) + \\ &\frac{\left(M\ln\left(K^F\lambda\right) + L\ln 2\right)}{\sqrt{2\pi M}} e^{\left(-\frac{\left(L\ln 2 - M\ln\left(K^F\lambda\right)\right)^2}{2M}\right)} - 2\Bigg). \end{aligned} \tag{32}$$

Next, by equating (32) to zero, one can get

$$\frac{\partial \bar{H}^{FS}_{LB}}{\partial M} = 0. \tag{33}$$

Then, one can obtain the root of above equation numerically as

$$M^* = \text{Root}\left(\frac{\partial \bar{H}^{FS}_{LB}}{\partial M} = 0\right) \tag{34}$$

where Root$(\cdot)$ means finding roots of the given equation. As there is no closed-form of M^* above, one may apply the bisection search method by setting lower and upper limit as M_{min} and M_{max}, respectively. Then, the optimal value of M can be approximated as

$$M^{FS} = \text{argmax}\left(\bar{H}_{LB}^{FS}(M)|M \in \{M_{max}, M_{min}, M^*\}\right) \tag{35}$$

IV. APEP AND ET UNDER 3D CHANNEL MODEL

In this section, we aim to derive the APEP under 3D channel model. Since we consider the 3D channel model, we introduce the minimum and maximum elevation angle $\Theta_{\min}$ and $\Theta_{\max}$, respectively, so that the UAV will not collide into nearby obstacles such as tall buildings and trees.

A. PDF and CDF of γ^{3D}

In that case, the APEP is given by

$$\bar{\varepsilon}^{3D} = \mathbb{E}\{\varepsilon(\gamma^{3D})\} = \int_{D_{min}}^{D_{max}} \int_{\Theta_{\min}}^{\Theta_{\max}} \varepsilon(\gamma^{3D}) f_{d,\theta}(x,y) dy dx, \tag{36}$$

where $f_{d,\theta}(x,y)$ is the joint PDF of d and θ, and γ in $\varepsilon(\gamma)$ is given in (10). Since the UAV is randomly deployed in the restricted space in Fig. 1, the PDF of θ is given by (5). In addition, since d and θ are independent, the joint PDF of d and θ are given by

$$f_{d,\theta}(x,y) = f_d(x) f_\theta(y) = \frac{1}{\Theta_{\max} - \Theta_{\min}} \frac{3x^2}{D_{\max}^3 - D_{\min}^3}. \tag{37}$$

The method developed for the free-space channel model cannot be adopted here since double integral needs to be calculated in (13).

Similar to Lemma 1, we derive the PDF of $\hat{d}$ in (10) as

$$f_{\hat{d}}(x) = \frac{3x^{-\frac{5}{2}}\tilde{C}^{3/2}}{2(D_{max}^3 - D_{min}^3)}, \hat{d}_{min} \le x \le \hat{d}_{max}, \tag{38}$$

where $\hat{d}_{min} = \frac{\tilde{C}}{D_{max}^2}$ and $\hat{d}_{min} = \frac{\tilde{C}}{D_{min}^2}$.

Lemma 3: The CDF of $\hat{\theta}$ can be given by

$$F_{\hat{\theta}}(x) = \frac{-\frac{\ln\left(\frac{\frac{\tilde{A}}{\ln(x)}-1}{a}\right)}{b} + a - \Theta_{\min}}{\Theta_{\max} - \Theta_{\min}}, \hat{\theta}_{min} \le \hat{\theta} \le \hat{\theta}_{max} \tag{39}$$

where $\hat{\theta}_{min} = \exp\left(\frac{\tilde{A}}{a\exp(-b(\Theta_{\min}-a))+1}\right)$ and $\hat{\theta}_{max} = \exp\left(\frac{\tilde{A}}{a\exp(-b(\Theta_{\max}-a))+1}\right)$.

Proof: Please refer to Appendix F. ■

By taking the first-order derivative of (39) with respect to $\hat{\theta}$, the PDF of $\hat{\theta}$ can be derived as

$$f_{\hat{\theta}}(x) = \frac{\tilde{A}}{bx(\Theta_{\max}-\Theta_{\min})\ln^2(x)\left(\frac{\tilde{A}}{\ln(x)}-1\right)}, \hat{\theta}_{min} \leq \hat{\theta} \leq \hat{\theta}_{max}. \tag{40}$$

Lemma 4: The PDF of γ^{3D} can be given by

$$f_{\gamma^{3D}}(z) = \begin{cases} W_1(z), & \hat{\theta}_{min}\cdot\hat{d}_{min} \leq z \leq \hat{\theta}_{min}\cdot\hat{d}_{max} \\ W_2(z), & \hat{\theta}_{min}\cdot\hat{d}_{max} \leq z \leq \hat{\theta}_{max}\cdot\hat{d}_{min} \\ W_3(z), & \hat{\theta}_{max}\cdot\hat{d}_{min} \leq z \leq \hat{\theta}_{max}\cdot\hat{d}_{max} \end{cases} \tag{41}$$

where $W_1(z)$, $W_2(z)$ and $W_3(z)$ are given by (65), (66) and (67), respectively.

Proof: Please refer to Appendix G. ■

B. Chebyshev Approximation

In this section, we provide the Chebyshev Approximation to $\bar{\varepsilon}^{3D}$. By using (41), one can get

$$\begin{aligned} \bar{\varepsilon}^{3D} = \mathbb{E}\{\varepsilon(\gamma^{3D})\} &= \int_{\hat{\theta}_{min}\cdot\hat{d}_{min}}^{\hat{\theta}_{min}\cdot\hat{d}_{max}} \varepsilon(z)W_1(z)dz \\ &+ \int_{\hat{\theta}_{min}\cdot\hat{d}_{max}}^{\hat{\theta}_{max}\cdot\hat{d}_{min}} \varepsilon(z)W_2(z)dz + \int_{\hat{\theta}_{max}\cdot\hat{d}_{min}}^{\hat{\theta}_{max}\cdot\hat{d}_{max}} \varepsilon(z)W_3(z)dz \end{aligned} \tag{42}$$

Let $q_1^{3D}(z) = \varepsilon(z)W_1(z)$, $q_2^{3D}(z) = \varepsilon(z)W_2(z)$ and $q_3^{3D}(z) = \varepsilon(z)W_3(z)$, one can have

$$\begin{aligned} \bar{\varepsilon}^{3D} \approx &\sum_{i=1}^{N} a_i \cdot q_1^{3D}\left(\frac{\hat{\theta}_{min}\cdot\hat{d}_{max}-\hat{\theta}_{min}\cdot\hat{d}_{min}}{2}t_i + \frac{\hat{\theta}_{min}\cdot\hat{d}_{max}+\hat{\theta}_{min}\cdot\hat{d}_{min}}{2}\right) + \sum_{i=1}^{N} a_i \cdot q_2^{3D}\cdot \\ &\left(\frac{\hat{\theta}_{max}\cdot\hat{d}_{min}-\hat{\theta}_{min}\cdot\hat{d}_{max}}{2}t_i + \frac{\hat{\theta}_{max}\cdot\hat{d}_{min}+\hat{\theta}_{min}\cdot\hat{d}_{max}}{2}\right) \\ &+ \sum_{i=1}^{N} a_i \cdot q_3^{3D}\left(\frac{\hat{\theta}_{max}\cdot\hat{d}_{min}-\hat{\theta}_{max}\cdot\hat{d}_{min}}{2}t_i + \frac{\hat{\theta}_{max}\cdot\hat{d}_{min}+\hat{\theta}_{max}\cdot\hat{d}_{min}}{2}\right). \end{aligned} \tag{43}$$

One can see that with the increase of N, the accuracy of the above expression will be increased, but at the cost of more computations. Then, by using (12) and (43), one can obtain the ET as

$$\bar{H}_C^{3D} = R_s\left(1-\bar{\varepsilon}^{3D}\right). \tag{44}$$

C. Lower Bound

Similarly, the lower bound of APEP can be given by

$$\bar{\varepsilon}^{3D} = \mathbb{E}\{\varepsilon(\gamma^{3D})\} \geq \varepsilon(\mathbb{E}\{\gamma^{3D}\}) \triangleq \bar{\varepsilon}^{3D}_{\mathrm{LB}}. \tag{45}$$

Then $\mathbb{E}\{\gamma^{3D}\}$ can be given by

$$\bar{\varepsilon}^{3D}_{\mathrm{LB}} = \varepsilon(U_1 + U_2 + U_3), \tag{46}$$

where U_1, U_2 and U_3 are given by (69), (70) and (71), respectively.

Proof: Please refer to Appendix H. ■

Similarly, ET can be expressed as

$$\bar{H}^{3D}_{LB} = R_s\left(1 - \bar{\varepsilon}^{3D}_{LB}\right) = R_s\left(1 - \varepsilon\left(U_1 + U_2 + U_3\right)\right). \tag{47}$$

Remark 4: When $\tilde{C} \gg 1$, i.e., $P/\sigma^2 \gg 1$, one can have $\bar{H}^{3D}_{LB} \to R_s$.

Proof: Please refer to Appendix I. ■

D. Throughput Maximization

In this section, we consider the throughput maximization under the latency constraint as follows

$$\begin{aligned} \mathcal{P}1: \ & \max_{M} \quad \bar{H}^{3D} \\ & \text{subject to}: M_{min} \leq M \leq M_{max}. \end{aligned} \tag{48}$$

One can see that the above problem can be transferred to

$$\begin{aligned} & \max_{M} \quad \bar{H}^{3D}_{LB} \\ & \text{subject to}: M_{min} \leq M \leq M_{max} \end{aligned} \tag{49}$$

By taking the first-order derivative of $\bar{H}^{3D}_{LB}$ with respect to M and equate the result to zero, one can get

$$\frac{\partial \bar{H}^{3D}_{LB}}{\partial M} = 0 \tag{50}$$

Then, one can obtain the root of above equation numerically as

$$M^* = \mathrm{Root}\left(\frac{\partial \bar{H}^{3D}_{LB}}{\partial M} = 0\right) \tag{51}$$

It is very difficult to obtain the closed-form solution of M^*. Therefore, similar with before, one may apply the bisection search method by setting the lower and upper limit as M_{min} and M_{max}, respectively. Then, the optimal value of M can be approximated as

$$M^{3D} = \text{argmax}\left(\bar{H}_{LB}^{3D}(M)|M \in \{M_{max}, M_{min}, M^*\}\right). \quad (52)$$

V. Numerical Results

In this section, simulation results are presented to verify the correctness of our derived results in this paper. Unless otherwise stated, the simulation parameters are set as follows: $D_{min} = 900$ m, $D_{max} = 950$ m, $B = 1$ MHz, $L = 500$ and $\sigma^2 = -173$ dBm/Hz. In FS scenario, we set $\beta = -40$ dB. In 3D case, we set $f_c = 2.5$ GHz, $c = 3 \cdot 10^8$ m/s and $\Theta_{\max} = 90$. Two scenarios are considered: dense urban and suburban. The values of the corresponding parameters can be found in [21]. $\Theta_{\min}$ is set to be 70 and 30 for dense urban and suburban, respectively. The other parameters are specified in each simulation figure. The curve labelled 'Simulation' is obtained by randomly and uniformly deploying the UAV in the specified region for 10000 times. The curve labelled 'Chebyshev' is obtained by using (19) in FS and (43) in 3D scenario. The curve labelled 'Upper' is obtained by using (28) in FS. Also, the curve labelled 'Lower' is obtained by using (23) in FS and (46) in 3D scenario.

A. FS Channel Model

In Fig. 2, we plot the APEP versus P in Fig. 2 (a) with the packet length given by $M = 100$, and APEP versus M in Fig. 2 (b) with the power given by $P = -5$ dBm. It is observed from Fig. 2 (a) that the APEP with finite blocklength regime decreases with the increase of P as expected. Also, one can see from Fig. 2 (b) that the APEP decreases with the increase of M as well, which confirms the conclusion from Remark 1. From Fig. 2, one can also see that our derived Chebyshev approximation result approximates the exact result very well. Also, the derived lower bound and upper bound results have similar performance as the exact curve. Hence, these results can be used to analyse the trend of the APEP. When the SNR value P is set to 5 dBm, the APEP can be as low as 10^{-16}. Also, it is noted that when the packet length M reaches 200, APEP can be as low as 10^{-7}, which satisfies the extremely reliability requirement for control signal transmission.

In Fig. 3, we plot the ET versus P in Fig. 3 (a) with the packet length given by $M = 100$, and ET versus M in Fig. 3 (b) with the power given by $P = -5$ dBm. One can see from Fig. 3

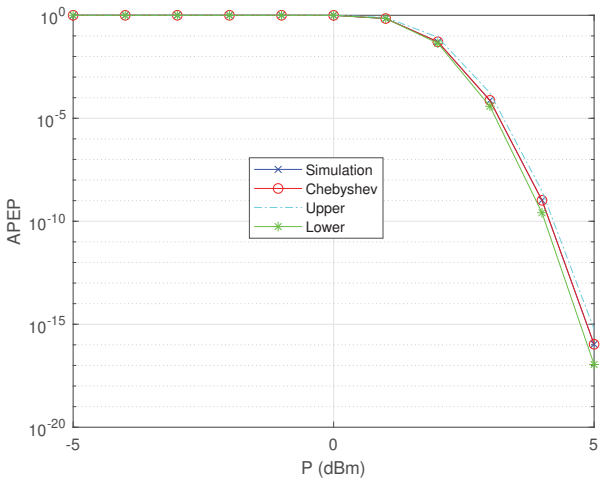

(a) APEP versus P with $M = 100$

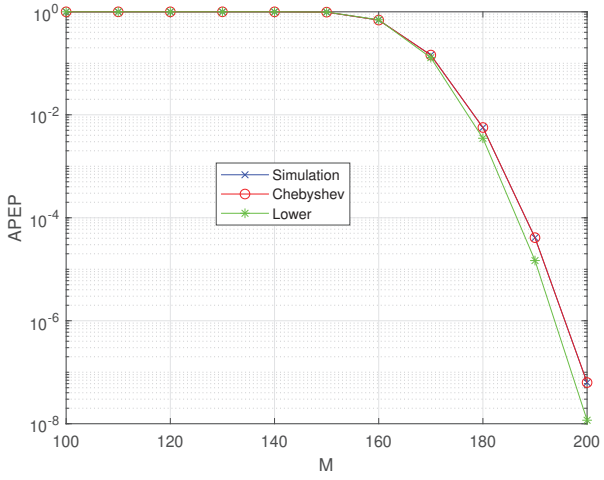

(b) APEP versus M with $P = -5$ dBm

Fig. 2: APEP in FS channel model

(a) that the ET increase with the increase of P, as expected. Also, one can see that the value of ET reaches the roof, i.e., $R_s = 3.47$ with the further increase of P, which can also be derived from Remark 2.

In Fig. 3 (b), one can see that ET first increases and then decreases with the increase of M. The maximal value can be reached when M is around 180. From (35), one can obtain M^{FS} numerically as $M^{FS} = 188.432$.

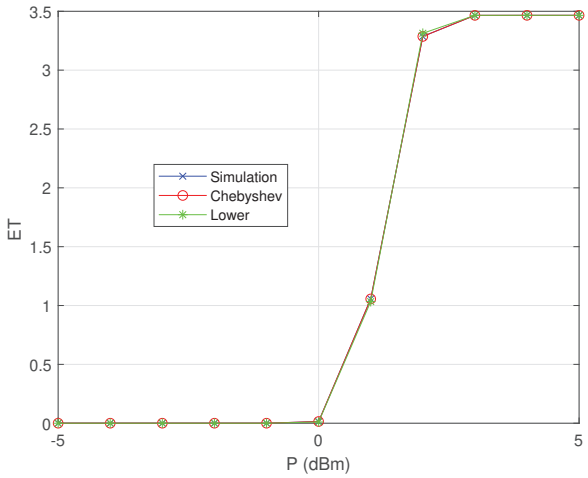

(a) ET versus P with $M = 100$

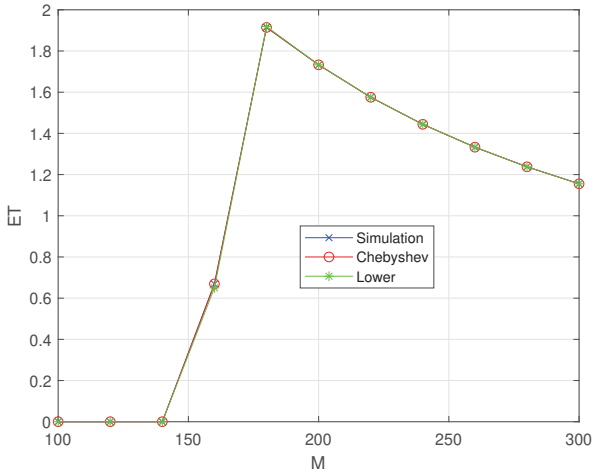

(b) ET versus M with $P = -5$ dBm

Fig. 3: ET in FS channel model

B. 3D Channel Model

In Fig. 4, we plot the APEP versus P in 3D scenario with the packet length $M = 100$, where Fig. 4 (a) shows suburban area while Fig. 4 (b) shows dense urban area. One can see that the APEP increase with the increase of P for both suburban and dense urban cases, as expected. Also, one can see in dense urban areas, we have worse APEP performance compared with suburban case.

In Fig. 5, we plot the APEP versus M in 3D scenario with the power of $P = -5$ dBm, where Fig. 5 (a) shows suburban area while Fig. 5 (b) shows dense urban area. One can see that the

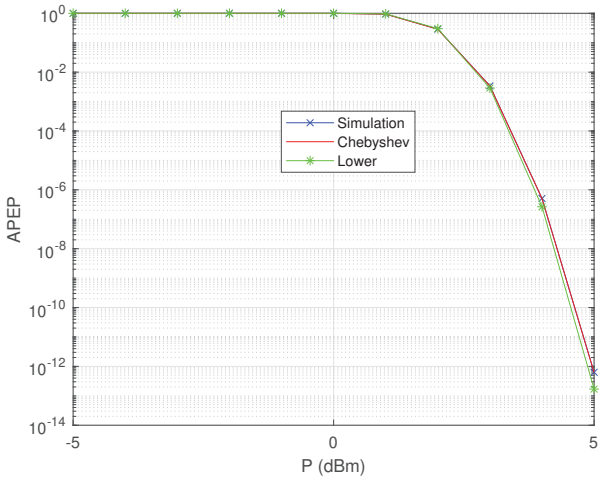

(a) Suburban

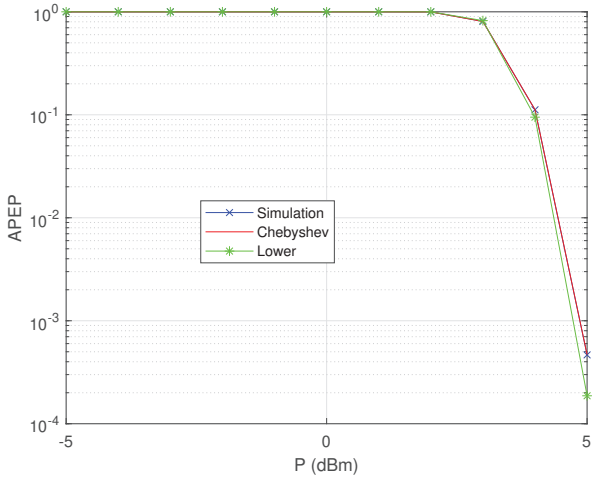

(b) Dense Urban

Fig. 4: APEP versus P with $M = 100$

APEP increases with the increase of M for both suburban and dense urban cases, as expected. Also, one can see in dense urban areas, we have worse APEP compared with suburban case.

In Fig. 6, we plot the ET versus P in 3D scenario with the packet length $M = 100$, where Fig. 6 (a) shows suburban area while Fig. 6 (b) shows dense urban area. One can see that the ET increase with the increase of P for both suburban and dense urban cases, as expected. Also, one can see in dense urban areas, we have worse ET compared with suburban area in the same parameter settings.

Also, one can see with the increase of P, ET reaches its upper floor 3.47 for both cases,

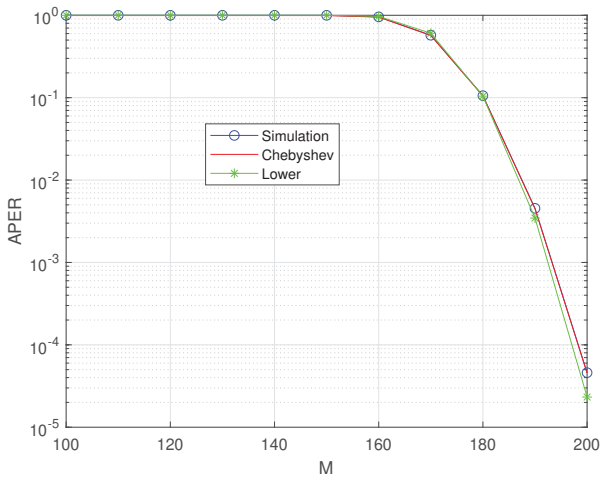

(a) Suburban

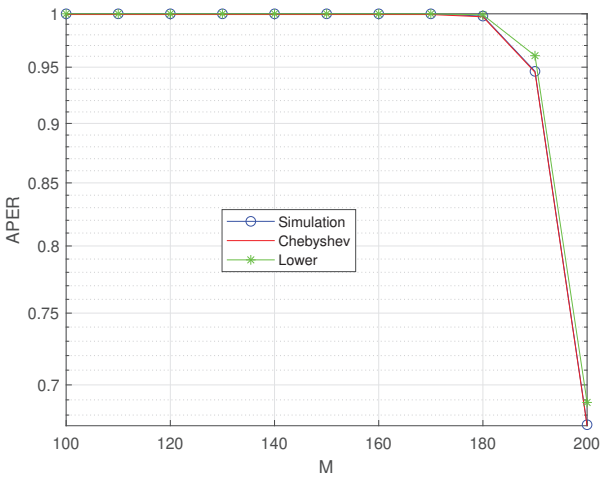

(b) Dense Urban

Fig. 5: APEP versus M with $P = -5$ dBm

which verifies Remark 6.

In Fig. 7, we plot the ET versus M in 3D scenario with the power of $P = -5$ dBm, where Fig. 7 (a) shows suburban area while Fig. 7 (b) shows dense urban area. One can see that ET first increases and then decreases with the increase of M for both cases. The maximal value can be reached when M is around 190 for suburban and 210 for dense urban scenarios. From (52), one can approximately get M^{3D} as $M^{3D} = 178.37$ for suburban scenario and $M^{3D} = 186.95$ for dense urban scenario.

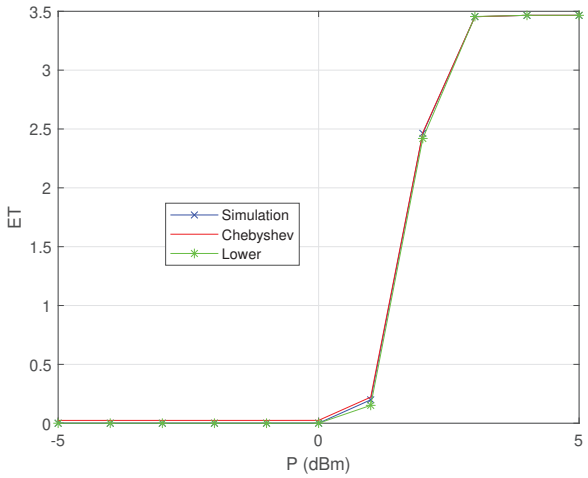

(a) Suburban

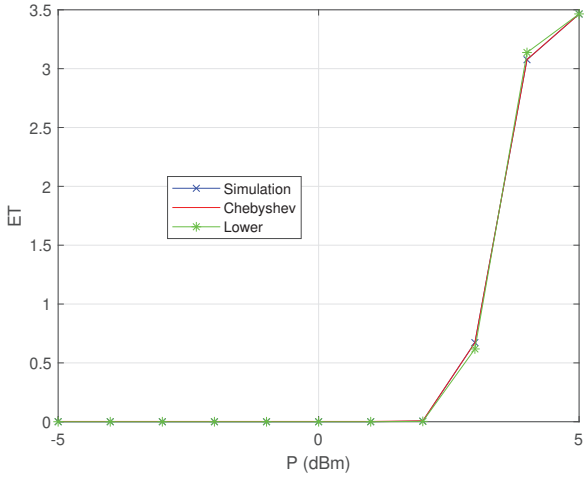

(b) Dense Urban

Fig. 6: ET versus P with $M = 100$

VI. Conclusions

In this paper, we have studied the APEP and ET for a GCS-to-UAV control link transmission under the short packet transmission regime to enable the stringent latency and reliable requirements. For the general scenario in FS and 3D, we have derived an accurate approximate expression of the APEP and ET by using the Gaussian-Chebyshev quadrature method. To obtain more insights, lower bound of APEP and ET for both FS and 3D scenarios have been derived. Moreover, the sub-optimal value of packet length with the objective of maximizing the ET has been obtained numerically.

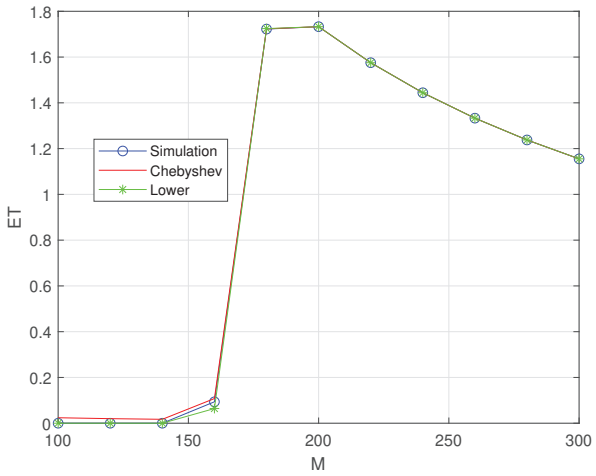

(a) Suburban

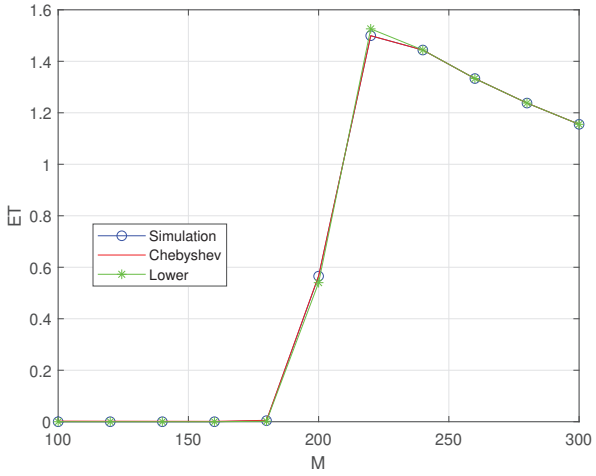

(b) Dense Urban

Fig. 7: ET versus M with $P = -5$ dBm

APPENDIX A
PROOF OF LEMMA 1

The CDF of γ can be given by [14]

$$F_{\gamma^{FS}}(x) = \Pr\{\gamma^{FS} \leq x\} = 1 - \Pr\left\{d \leq \left(\frac{\lambda}{x}\right)^{1/2}\right\}. \tag{53}$$

By applying (1) and (53), the CDF of γ^{FS} can be obtained as follows

$$F_{\gamma^{FS}}(x)=\begin{cases} 1-\frac{(\frac{\lambda}{x})^{3/2}-D_{min}^{3}}{D_{max}^{3}-D_{min}^{3}}, \gamma_{min}^{FS}\leq x\leq\gamma_{max}^{FS} \\ 0, \qquad\qquad \text{otherwise} \end{cases}. \tag{54}$$

By taking the first-order derivative of (54), the PDF of γ^{FS} can be derived as (15).

APPENDIX B
PROOF OF LEMMA 2

$\varepsilon(\gamma^{+})$ defined in (11) can be regarded as a composition function of Q-function and f-function. For the Q-function $Q\left(x\right)=\frac{1}{\sqrt{2\pi}}\int_{x}^{\infty}e^{-\frac{t^{2}}{2}}\mathrm{d}t$, the first-order derivative of $Q\left(x\right)$ w.r.t. x can be calculated as $Q'\left(x\right)=-\frac{1}{\sqrt{2\pi}}e^{-\frac{x^{2}}{2}}<0$, and the second-order derivative is $Q''\left(x\right)=\frac{x}{\sqrt{2\pi}}e^{-\frac{x^{2}}{2}}>0$ when $x>0$. For URLLC applications, the decoding error probability is generally much smaller than 0.5, which is equal to $Q(0)$. Since $Q(x)$ is a decreasing function, $x>0$ always holds. Hence, $Q(x)$ is a decreasing and convex function w.r.t. x. According to the composition rules in [22], $\varepsilon(\gamma^{+})$ is a convex function of γ^{+} if $f\left(\gamma^{+}\right)$ is a concave function of γ^{+}, which will be proved in the following.

The first-order derivative of $f\left(\gamma^{+}\right)$ w.r.t. γ^{+} is given by

$$f'\left(\gamma^{+}\right)=\sqrt{M}\frac{\left(1+\gamma^{+}\right)^{2}-1-\left(\ln\left(1+\gamma^{+}\right)-\frac{L}{M}\ln 2\right)}{\left(\left(1+\gamma^{+}\right)^{2}-1\right)^{\frac{3}{2}}} \tag{55}$$

The second-order derivative of $f\left(\gamma^{+}\right)$ w.r.t. γ^{+} can be calculated as

$$f''\left(\gamma^{+}\right)=\frac{\sqrt{M}}{\left(\left(1+\gamma^{+}\right)^{2}-1\right)^{\frac{5}{2}}}g\left(\gamma^{+}\right). \tag{56}$$

where function $g\left(\gamma^{+}\right)$ is given by

$$g\left(\gamma^{+}\right)=\left(-\left(1+\gamma^{+}\right)-\frac{1}{1+\gamma^{+}}\right)\left(\left(1+\gamma^{+}\right)^{2}-1\right)+3\left(1+\gamma^{+}\right)\left(\ln\left(1+\gamma^{+}\right)-\frac{L}{M}\ln 2\right). \tag{57}$$

Hence, we need to check the sign of function $g\left(\gamma^{+}\right)$. The first-order derivative of $g\left(\gamma^{+}\right)$ w.r.t. γ^{+} is given by

$$g'\left(\gamma^{+}\right)=-3(1+\gamma^{+})^{2}-\frac{1}{(1+\gamma^{+})^{2}}+3\left(\ln\left(1+\gamma^{+}\right)-\frac{L}{M}\ln 2\right)+3. \tag{58}$$

The second-order derivative of $g\left(\gamma^{+}\right)$ w.r.t. γ^{+} is

$$g''\left(\gamma^{+}\right)=\frac{h(\gamma^{+})}{\left(1+\gamma^{+}\right)^{3}}, \tag{59}$$

where $h(\gamma^{+})=-6(1+\gamma^{+})^{4}+2+3(1+\gamma^{+})^{2}$. The first-order derivative of $h(\gamma^{+})$ w.r.t. γ^{+} is given by $h'(\gamma^{+})=6(1+\gamma^{+})\left(1-4(1+\gamma^{+})^{2}\right)$, which is smaller than zero. Hence, $h(\gamma^{+})$ is a monotonically decreasing function. We then have $h(\gamma^{+})<h(0)=-1$. Then, according to (59), we have $g''\left(\gamma^{+}\right)<0$, which means $g'\left(\gamma^{+}\right)$ is also a monotonically decreasing function. Hence, we have $g'\left(\gamma^{+}\right)<g'\left(0\right)=-\frac{L}{M}3\ln 2-1<0$. Again, this means $g(\gamma^{+})$ is also a monotonically decreasing function. Then, we have $g(\gamma^{+})<g(0)=-\frac{L}{M}3\ln 2<0$. By substituting the relation $g(\gamma^{+})<0$ into (56), we can prove that $f''\left(\gamma^{+}\right)<0$, which means $f\left(\gamma^{+}\right)$ is a concave function, which completes the proof.

Appendix C
Proof of Remark 1

When $x\gg 1$, one has the following approximation

$$\log(1+x)\approx\log(x), \tag{60}$$

and

$$\sqrt{V(x)}=\sqrt{1-\frac{1}{(x+1)^{2}}}\approx 1. \tag{61}$$

By using above two approximations, (23) can be written as (25).

Appendix D
Proof of Remark 2

When $\lambda\gg 1$, similar with before, $\bar{H}_{LB}^{FS}$ in (24) can be written as

$$\bar{H}_{LB}^{FS}=R_{s}\left(1-\frac{1}{2}\text{erfc}\left(\sqrt{M/2}\left(\ln\left(K^{F}\lambda\right)-R_{s}\right)\right)\right). \tag{62}$$

By using $\text{erf}(x)\to 1$ when $x\to\infty$ and $\text{erfc}(x)=1-\text{erf}(x)$, one can get $\bar{H}_{LB}^{FS}\to R_{s}$, which completes the proof.

APPENDIX E
PROOF OF REMARK 3

In the case of $x \to \infty$ in (27), one has $\text{erf}(x) \to 1$. Therefore, $u(x)$ can be approximated as

$$u(x) \approx -\frac{2\text{erfc}\left(\frac{M\ln(x)-L\ln(2)}{\sqrt{2}\sqrt{M}}\right)}{3x^{3/2}} - \frac{2}{3}e^{\frac{(L\ln(4)-3)^2-4L^2\ln^2(2)}{8M}}.$$

Then, after some simple manipulations, one can get (28).

APPENDIX F
PROOF OF LEMMA 3

The CDF of $\hat{\theta}$ can be given by

$$F_{\hat{\theta}}(x) = \Pr\{e^{\frac{\tilde{A}}{1+a\exp(-b(\theta-a))}} \leq x\}. \tag{63}$$

Similar to Appendix A and by applying $F_\theta(x)$ in (6), the CDF of $\hat{\theta}$ can be obtained as (39).

APPENDIX G
PROOF OF LEMMA 4

Without loss of generality, we assume that $\hat{\theta}_{min}\cdot\hat{d}_{max} \leq z \leq \hat{\theta}_{max}\cdot\hat{d}_{min}$ in the next derivations. For the cases of $\hat{\theta}_{min}\cdot\hat{d}_{max} = z \leq \hat{\theta}_{max}\cdot\hat{d}_{min}$ or $\hat{\theta}_{min}\cdot\hat{d}_{max} = z \geq \hat{\theta}_{max}\cdot\hat{d}_{min}$, similar derivations can be used which are omitted here due to space limitation.

By using $f_{\hat{d}}(x)$ in (38) and $f_{\hat{\theta}}(x)$ in (40) and [23], one can get the PDF of γ^{3D} as

$$f_{\gamma^{3D}}(z) = \begin{cases} W_1(z) = \int_{\hat{\theta}_{min}}^{z/\hat{d}_{min}} f_{\hat{\theta}}(x) f_{\hat{d}}(\frac{z}{x})\frac{1}{x}dx, \hat{\theta}_{min}\cdot\hat{d}_{min} \leq z \leq \hat{\theta}_{min}\cdot\hat{d}_{max}; \\ W_2(z) = \int_{z/\hat{d}_{max}}^{z/\hat{d}_{min}} f_{\hat{\theta}}(x) f_{\hat{d}}(\frac{z}{x})\frac{1}{x}dx, \hat{\theta}_{min}\cdot\hat{d}_{max} \leq z \leq \hat{\theta}_{max}\cdot\hat{d}_{min}; \\ W_3(z) = \int_{z/\hat{d}_{max}}^{\hat{\theta}_{max}} f_{\hat{\theta}}(x) f_{\hat{d}}(\frac{z}{x})\frac{1}{x}dx, \hat{\theta}_{max}\cdot\hat{d}_{min} \leq z \leq \hat{\theta}_{max}\cdot\hat{d}_{max}. \end{cases} \tag{64}$$

For $W_1(z)$, by using the variable substitution and [20], [24], one can have

$$\begin{aligned} W_1(z) &= \int_{\hat{\theta}_{min}}^{z/\hat{d}_{min}} f_{\hat{\theta}}(x) f_{\hat{d}}(\frac{z}{x})\frac{1}{x}dx = \\ &\frac{3\tilde{A}\tilde{C}^{3/2}z^{-5/2}}{2b\left(D_{max}^3 - D_{min}^3\right)\left(\Theta_{\max}-\Theta_{\min}\right)} \int_{\hat{\theta}_{min}}^{z/\hat{d}_{min}} \frac{\sqrt{x}dx}{\tilde{A}\ln(x) - \ln^2(x)} \\ &= \frac{3\tilde{C}^{3/2}z^{-5/2}}{2b\left(D_{max}^3 - D_{min}^3\right)\left(\Theta_{\max}-\Theta_{\min}\right)} \left(g(\frac{z}{\hat{d}_{min}}) - g(\hat{\theta}_{min})\right) \end{aligned} \tag{65}$$

where $g(x) = \text{Ei}\left(\frac{3\ln(x)}{2}\right) - e^{\frac{3\tilde{A}}{2}}\text{Ei}\left(\frac{3}{2}(\ln(x) - \tilde{A})\right)$ and Ei gives the exponential integral function, defined by $\text{Ei}(z) = -\int_{-z}^{\infty} \frac{e^{-t}}{t}\, dt$ [20].

Similarly, one can get $W_2(z)$ as

$$W_2(z) = \frac{3\tilde{C}^{3/2} z^{-5/2}}{2b\left(D_{max}^3 - D_{min}^3\right)\left(\Theta_{\max} - \Theta_{\min}\right)} \cdot \left(g(z/\hat{d}_{min}) - g(z/\hat{d}_{max})\right). \tag{66}$$

Also, one can get $W_3(z)$ as

$$W_3(z) = \frac{3\tilde{C}^{3/2} z^{-5/2}}{2b\left(D_{max}^3 - D_{min}^3\right)\left(\Theta_{\max} - \Theta_{\min}\right)} \cdot \left(g(\hat{\theta}_{\max}) - g(z/\hat{d}_{max})\right). \tag{67}$$

Then, one can obtain the PDF of γ^{3D} as (41).

Appendix H
Proof of (46)

$\mathbb{E}\{\gamma^{3D}\}$ can be written as

$$\mathbb{E}\{\gamma^{3D}\} = \underbrace{\int_{\hat{\theta}_{min}\cdot\hat{d}_{min}}^{\hat{\theta}_{min}\cdot\hat{d}_{max}} z W_1(z) dz}_{U_1} + \underbrace{\int_{\hat{\theta}_{min}\cdot\hat{d}_{max}}^{\hat{\theta}_{max}\cdot\hat{d}_{min}} z W_2(z) dz}_{U_2} + \underbrace{\int_{\hat{\theta}_{max}\cdot\hat{d}_{min}}^{\hat{\theta}_{max}\cdot\hat{d}_{max}} z W_3(z) dz}_{U_3}. \tag{68}$$

By using $W_1(z)$ in (65), one can have U_1 as [20], [25]

$$\begin{aligned} U_1 = {} & \frac{3\tilde{C}^{3/2}}{2b\left(D_{max}^3 - D_{min}^3\right)\left(\Theta_{\max} - \Theta_{\min}\right)} \cdot \\ & \Bigg(\underbrace{\int_{\hat{\theta}_{min}\cdot\hat{d}_{min}}^{\hat{\theta}_{min}\cdot\hat{d}_{max}} z^{-3/2}\text{Ei}\left(\frac{3}{2}\ln\left(\frac{zD_{max}^2}{\tilde{C}}\right)\right) dz}_{U_{11}} - \\ & \underbrace{\int_{\hat{\theta}_{min}\cdot\hat{d}_{min}}^{\hat{\theta}_{min}\cdot\hat{d}_{max}} e^{\frac{3\tilde{A}}{2}} z^{-3/2}\text{Ei}\left(\frac{-3}{2}\left(\tilde{A} - \ln\left(\frac{z{D_{max}}^2}{\tilde{C}}\right)\right)\right) dz}_{U_{12}} - \\ & \underbrace{\int_{\hat{\theta}_{min}\cdot\hat{d}_{min}}^{\hat{\theta}_{min}\cdot\hat{d}_{max}} z^{\frac{-3}{2}}\text{Ei}\left(\frac{3}{2}\ln\left(e^{\frac{\tilde{A}}{a\exp(-b(\Theta_{\min}-a))+1}}\right)\right) dz}_{U_{13}} + \\ & \underbrace{\int_{\hat{\theta}_{min}\cdot\hat{d}_{min}}^{\hat{\theta}_{min}\cdot\hat{d}_{max}} e^{\frac{3\tilde{A}}{2}} z^{\frac{-3}{2}}\text{Ei}\left(\frac{-3}{2}\left(\tilde{A} - \ln\left(e^{\frac{\tilde{A}}{a\exp(-b(\Theta_{\min}-a))+1}}\right)\right)\right) dz}_{U_{14}} \Bigg) \end{aligned} \tag{69}$$

Then, by using [20], [25], for U_{11} above, one can have $U_{11} = L_{11}(\hat{\theta}_{min}\cdot\hat{d}_{max}) - L_{11}(\hat{\theta}_{min}\cdot\hat{d}_{min})$, where $L_{11}(z) = -\frac{2}{\sqrt{z}}(\text{Ei}(\frac{3}{2}\ln(\frac{D_{max}^2 z}{\tilde{C}})) - \sqrt{\frac{D_{max}^2 z}{\tilde{C}}}\text{li}(\frac{D_{max}^2 z}{\tilde{C}}))$ and $\text{li}(z) = \int_0^z \frac{dt}{\log t}$ denotes the logarithmic integral function [20]; for U_{12}, one can have $U_{12} = L_{12}(\hat{\theta}_{min}\cdot\hat{d}_{max}) - L_{12}(\hat{\theta}_{min}\cdot\hat{d}_{min})$,

where $L_{12}(z) = \frac{2}{\sqrt{z}} e^{\frac{3\tilde{A}}{2}} (e^{-\frac{\tilde{A}}{2}} \sqrt{\frac{D_{max}^2 z}{\tilde{C}}} \text{Ei}(\ln(\frac{D_{max}^2 z}{\tilde{C}}) - \tilde{A}) - \text{Ei}(\frac{-3}{2}(\tilde{A} - \ln(\frac{D_{max}^2 z}{\tilde{C}}))))$; for U_{13}, one can have $U_{13} = L_{13}(\hat{\theta}_{min} \cdot \hat{d}_{max}) - L_{13}(\hat{\theta}_{min} \cdot \hat{d}_{min})$, where $L_{13}(z) = -\frac{2}{\sqrt{z}} \text{Ei}(\frac{3}{2} \ln(e^{\frac{\tilde{A}}{e^{b(a-\Theta_{\min})a+1}}}))$ and for U_{14}, one can have $U_{14} = L_{14}(\hat{\theta}_{min} \cdot \hat{d}_{max}) - L_{14}(\hat{\theta}_{min} \cdot \hat{d}_{min})$, where $L_{14}(z) = -\frac{2}{\sqrt{z}} e^{\frac{3\tilde{A}}{2}} \text{Ei}(\frac{-3}{2}(\tilde{A} - \ln(e^{\frac{\tilde{A}}{e^{b(a-\Theta_{\min})a+1}}})))$.

Similarly, for U_2, one can have

$$U_2 = \frac{3\tilde{C}^{3/2}}{2b\left(D_{max}^3 - D_{min}^3\right)\left(\Theta_{\max} - \Theta_{\min}\right)} \cdot (U_{21} + U_{22} + U_{23} + U_{24}) \tag{70}$$

where $U_{21} = L_{21}(\hat{\theta}_{max} \cdot \hat{d}_{min}) - L_{21}(\hat{\theta}_{min} \cdot \hat{d}_{max})$, $U_{22} = L_{22}(\hat{\theta}_{max} \cdot \hat{d}_{min}) - L_{22}(\hat{\theta}_{min} \cdot \hat{d}_{max})$, $U_{23} = L_{23}(\hat{\theta}_{max} \cdot \hat{d}_{min}) - L_{23}(\hat{\theta}_{min} \cdot \hat{d}_{max})$, $U_{24} = L_{24}(\hat{\theta}_{max} \cdot \hat{d}_{min}) - L_{24}(\hat{\theta}_{min} \cdot \hat{d}_{max})$, $L_{21}(z) = -\frac{2}{\sqrt{z}}(\text{Ei}(\frac{3}{2} \ln(\frac{D_{max}^2 z}{\tilde{C}})) - \sqrt{\frac{D_{max}^2 z}{\tilde{C}}} \text{li}(\frac{D_{max}^2 z}{\tilde{C}}))$, $L_{22}(z) = \frac{2}{\sqrt{z}} e^{\frac{3\tilde{A}}{2}} [e^{-\frac{\tilde{A}}{2}} \sqrt{\frac{D_{max}^2 z}{\tilde{C}}} \text{Ei}(\ln(\frac{{D_{max}}^2 z}{\tilde{C}}) - \tilde{A}) - \text{Ei}(\frac{-3}{2}(\tilde{A} - \ln(\frac{{D_{max}}^2 z}{\tilde{C}})))]$, $L_{23}(z) = -\frac{2}{\sqrt{z}}(\text{Ei}(\frac{3}{2} \ln(\frac{D_{min}^2 z}{\tilde{C}})) - \sqrt{\frac{D_{min}^2 z}{\tilde{C}}} \text{li}(\frac{D_{min}^2 z}{\tilde{C}}))$ and $L_{24}(z) = \frac{2}{\sqrt{z}} e^{\frac{3\tilde{A}}{2}} [e^{-\frac{\tilde{A}}{2}} \sqrt{\frac{D_{min}^2 z}{\tilde{C}}} \text{Ei}(\ln(\frac{{D_{min}}^2 z}{\tilde{C}}) - \tilde{A}) - \text{Ei}(\frac{-3}{2}(\tilde{A} - \ln(\frac{D_{min}^2 z}{\tilde{C}})))]$.

Similarly, for U_3, one can have

$$U_3 = \frac{3\tilde{C}^{3/2}}{2b\left(D_{max}^3 - D_{min}^3\right)\left(\Theta_{\max} - \Theta_{\min}\right)} \cdot (U_{31} + U_{32} + U_{33} + U_{34}) \tag{71}$$

where $U_{31} = L_{31}(\hat{\theta}_{max} \cdot \hat{d}_{max}) - L_{31}(\hat{\theta}_{max} \cdot \hat{d}_{min})$, $U_{32} = L_{32}(\hat{\theta}_{max} \cdot \hat{d}_{max}) - L_{32}(\hat{\theta}_{max} \cdot \hat{d}_{min})$, $U_{33} = L_{33}(\hat{\theta}_{max} \cdot \hat{d}_{max}) - L_{33}(\hat{\theta}_{max} \cdot \hat{d}_{min})$, $U_{34} = L_{34}(\hat{\theta}_{max} \cdot \hat{d}_{max}) - L_{34}(\hat{\theta}_{max} \cdot \hat{d}_{min})$, $L_{31}(z) = -\frac{2}{\sqrt{z}} \text{Ei}(\frac{3}{2} \ln(e^{\frac{\tilde{A}}{e^{b(a-\Theta_{\max})a+1}}}))$, $L_{32}(z) = -\frac{2}{\sqrt{z}} e^{\frac{3\tilde{A}}{2}} \text{Ei}(\frac{-3}{2}(\tilde{A} - \ln(e^{\frac{\tilde{A}}{e^{b(a-\Theta_{\max})a+1}}})))$, $L_{33}(z) = -\frac{2}{\sqrt{z}}(\text{Ei}(\frac{3}{2} \ln(\frac{D_{min}^2 z}{\tilde{C}})) - \sqrt{\frac{D_{min}^2 z}{\tilde{C}}} \text{li}(\frac{D_{min}^2 z}{\tilde{C}}))$ and $L_{34}(z) = \frac{2}{\sqrt{z}} e^{\frac{3\tilde{A}}{2}} [e^{-\frac{\tilde{A}}{2}} \sqrt{\frac{D_{min}^2 z}{\tilde{C}}} \text{Ei}(\ln(\frac{D_{min}^2 z}{\tilde{C}}) - \tilde{A}) - \text{Ei}(\frac{-3}{2}(\tilde{A} - \ln(\frac{D_{min}^2 z}{\tilde{C}})))]$.

APPENDIX I
PROOF OF REMARK 4

When $\tilde{C} \gg 1$, i.e., $P/\sigma^2 \gg 1$, similar with before, by using $\text{erf}(x) \to 1$ when $x \to \infty$ and $\text{erfc}(x) = 1 - \text{erf}(x)$, one can get $\bar{H}_{LB}^{3D} \to R_s$, which completes the proof.

REFERENCES

[1] Y. Zeng, R. Zhang, and T. J. Lim, "Wireless communications with unmanned aerial vehicles: opportunities and challenges," *IEEE Commun. Mag.,*, vol. 54, no. 5, pp. 36–42, May 2016.

[2] J. Wang, C. Jiang, Z. Han, Y. Ren, R. G. Maunder, and L. Hanzo, "Taking drones to the next level: Cooperative distributed unmanned-aerial-vehicular networks for small and mini drones," *IEEE Vehicular Technology Magazine*, vol. 12, no. 3, pp. 73–82, Sep. 2017.

[3] Y. Zeng, R. Zhang, and T. J. Lim, "Throughput maximization for UAV-enabled mobile relaying systems," *IEEE Transactions on Communications*, vol. 64, no. 12, pp. 4983–4996, Dec 2016.

[4] Y. Zeng and R. Zhang, "Energy-efficient UAV communication with trajectory optimization," *IEEE Transactions on Wireless Communications*, vol. 16, no. 6, pp. 3747–3760, June 2017.

[5] Q. Wu, Y. Zeng, and R. Zhang, "Joint trajectory and communication design for multi-UAV enabled wireless networks," *IEEE Transactions on Wireless Communications*, vol. 17, no. 3, pp. 2109–2121, March 2018.

[6] A. Al-Hourani, S. Kandeepan, and S. Lardner, "Optimal lap altitude for maximum coverage," *IEEE Wireless Communications Letters*, vol. 3, no. 6, pp. 569–572, Dec 2014.

[7] M. Mozaffari, W. Saad, M. Bennis, and M. Debbah, "Efficient deployment of multiple unmanned aerial vehicles for optimal wireless coverage," *IEEE Communications Letters*, vol. 20, no. 8, pp. 1647–1650, Aug 2016.

[8] M. Alzenad, A. El-Keyi, F. Lagum, and H. Yanikomeroglu, "3-D placement of an unmanned aerial vehicle base station (UAV-BS) for energy-efficient maximal coverage," *IEEE Wireless Communications Letters*, vol. 6, no. 4, pp. 434–437, Aug 2017.

[9] T. Bai, J. Wang, Y. Ren, and L. Hanzo, "Energy-efficient computation offloading for secure uav-edge-computing systems," *IEEE Transactions on Vehicular Technology*, vol. 68, no. 6, pp. 6074–6087, June 2019.

[10] C. She, C. Yang, and T. Q. S. Quek, "Cross-layer optimization for ultra-reliable and low-latency radio access networks," *IEEE Transactions on Wireless Communications*, vol. 17, no. 1, pp. 127–141, Jan 2018.

[11] C. She, C. Liu, T. Q. S. Quek, C. Yang, and Y. Li, "Ultra-reliable and low-latency communications in unmanned aerial vehicle communication systems," *IEEE Transactions on Communications*, vol. 67, no. 5, pp. 3768–3781, May 2019.

[12] C. Pan, H. Ren, Y. Deng, M. Elkashlan, and A. Nallanathan, "Joint blocklength and location optimization for URLLC-enabled UAV relay systems," *IEEE Communications Letters*, vol. 23, no. 3, pp. 498–501, March 2019.

[13] Y. Polyanskiy, H. V. Poor, and S. Verdu, "Channel coding rate in the finite blocklength regime," *IEEE Trans. Inf. Theory*, vol. 56, no. 5, pp. 2307–2359, May 2010.

[14] H. Ren, C. Pan, K. Wang, Y. Deng, M. Elkashlan, and A. Nallanathan, "Achievable data rate for URLLC-enabled UAV systems with 3-D channel model," *IEEE Wireless Communications Letters*, vol. 8, no. 6, pp. 1587–1590, Dec 2019.

[15] A. A. Khuwaja, Y. Chen, N. Zhao, M.-S. Alouini, and P. Dobbins, "A survey of channel modeling for uav communications," *IEEE Communications Surveys & Tutorials*, vol. 20, no. 4, pp. 2804–2821, 2018.

[16] C. E. Shannon, "A mathematical theory of communication," *Bell system technical journal*, vol. 27, no. 3, pp. 379–423, 1948.

[17] G. Durisi, T. Koch, and P. Popovski, "Toward massive, ultrareliable, and low-latency wireless communication with short packets," *Proc. IEEE*, vol. 104, no. 9, pp. 1711–1726, Sept 2016.

[18] M. Abramowitz and I. A. Stegun, *Handbook of Mathematical Functions with Formulas, Graphs, and Mathematical Tables, 9th ed.* Handbook of Mathematical Functions with Formulas, Graphs, and Mathematical Tables, 1972.

[19] Wolfram Research, Inc., "Complementary error function," http://functions.wolfram.com/GammaBetaErf/Erfc/21/01/02/04/01/.

[20] Wolfram Research, Inc., "Mathematica, Version 11.0." [Online]. Available: https://www.wolfram.com/mathematica

[21] R. I. Bor-Yaliniz, A. El-Keyi, and H. Yanikomeroglu, "Efficient 3-D placement of an aerial base station in next generation cellular networks," in *2016 IEEE ICC*. IEEE, 2016, pp. 1–5.

[22] S. Boyd and L. Vandenberghe, *Convex optimization*. Cambridge university press, 2004.

[23] A. G. Glen, L. M. Leemis, and J. H. Drew, "Computing the distribution of the product of two continuous random variables," *Computational statistics & data analysis*, vol. 44, no. 3, pp. 451–464, 2004.

[24] Wolfram Research, Inc., "Exponential function," http://functions.wolfram.com/ElementaryFunctions/Exp/21/01/02/02/02/.

[25] ——, "Expintegralei function," http://functions.wolfram.com/GammaBetaErf/ExpIntegralEi/21/01/.